Developing tools for assessing the Fluid Structure Interaction of Passive Adaptive Composite foils

L. Marimon Giovannetti, J. Banks, S. W. Boyd, S. R. Turnock
Faculty of Engineering and the Environment, Fluid Structures Interaction Group
University of Southampton, UK

ABSTRACT: The study presents an experimental and numerical evaluation of bend-twist elastic coupling in composite passive-adaptive structures. Due to the lack of experimental validation in Fluid Structure Interaction (FSI) investigations, a full-field deformation of an aerofoil-shaped section under wind loading is measured. The experimental analysis is carried out at the University of Southampton 3.5 m × 2.4 m R. J. Mitchell wind tunnel using full-field non-contact measurement techniques such as high speed three dimensional Digital Image Correlation (DIC) and stereoscopic Particle Image Velocimetry (PIV). After assessing the validity and repeatability of the experiments, the study focuses on the development of a numerical FSI investigation that involves the use of a structural and a fluid solver to simulate the aero-elastic behaviour of composite tailored structures with different lay-up arrangements. The numerical analysis is developed as a design tool to allow the structure investigated to maximise bend-twist coupling under increased aerodynamic loading.

1 INTRODUCTION

The recent developments in composite materials lead to their applications along a wide variety of different structures, from the aircraft industry, to renewable energy devices, to high performance sports applications and marine components. For many of these applications, the ability of a foil to passively adapt to the experienced fluid loading could be advantageous (De Goeij et al. 1999, Karaolis 1989, Nicholls-Lee et al. 2009, Shirk et al. 1985). Composite materials provide the opportunity to tailor the bend twist coupling of a structure to achieve these goals, accounting for the inherent flexibility of the composite laminates (Veers et al. 1998). In order to have a bend-twist coupling in the structure, the fibres at the opposite sides of the laminate shear centre should be oriented in the same direction. To allow such foils to be designed and assessed, numerical tools such as finite element analysis (FEA) and computational fluid dynamics (CFD) will need to be coupled together in fluid-structure interaction (FSI) simulations (Turnock and Wright 2000).

Even though numerical studies have been extensive, especially in recent years with the increase in computer power, there is a lack of experimental validation cases for FSI problems (Ducoin et al. 2012, Fedorov 2012, Malijaarsl and Kaminski 2015). Experimental and numerical investigations conducted on a flexible NACA0015 foil are presented. The experimental methodology within the working section of a wind tunnel was first developed at the University of Southampton (Banks et al. 2015). The numerical tools presented are validated against a well-known measurement technique (namely Digital Image Correlation) and the forces response measured by the wind tunnel balance. The two systems are synchronised to simultaneously assess the structural response and the fluid behaviour of a composite aerofoil. A complementary experimental and numerical FSI technique can be applied to, for example, the investigation of the tailored aero-elastic behaviour of wind turbine blades, tidal turbine blades, marine propellers and Formula 1 rear wings. All these components present similar shapes, with a possibility of improving their performances by utilising the inherent flexibility of composite materials and designing structures optimised for strength, rather than for stiffness. The efficiency of the foils can therefore be improved by tailoring the material to induce smart coupled bend-twist toward a wash-out (feather) or wash-in (stall) position under increased loading.

2 BACKGROUND ON PASSIVE ADAPTIVE COMPOSITES

Composite materials are defined as being made up of two or more constituent parts (Reddy 2000). Composite structures, designed to maximise their stiffness, are mostly symmetric laminates with fibres located at 0°, ±45° and 90°, therefore presenting quasi-isotropic material properties as the major loading modes are counteracted by the fibres positioned at those four characteristic angles.

However, if the laminate is not symmetric and is designed for its strength, allowing flexibility in the structure, the interactions between bending and/or extension coupling must be considered (Barbero 2008). Using the anisotropy of the material, it is possible to design components presenting elastic couplings that will enhance the performance of the whole structure (Fedorov 2012, Veers et al. 1998). In those structures, the relationship of the stresses and strains must take into consideration the complete stiffness matrix as the stresses (σ and τ) and strains (ϵ and γ) are coupled to σ_1 and/or σ_2 in the two principal directions, leading to:

$$\begin{bmatrix} \sigma_x \\ \sigma_y \\ \tau_{xy} \end{bmatrix} = \begin{bmatrix} \bar{Q}_{11} & \bar{Q}_{12} & \bar{Q}_{16} \\ \bar{Q}_{12} & \bar{Q}_{22} & \bar{Q}_{26} \\ \bar{Q}_{16} & \bar{Q}_{26} & \bar{Q}_{66} \end{bmatrix} \begin{bmatrix} \epsilon_x \\ \epsilon_y \\ \gamma_{xy} \end{bmatrix} \quad (1)$$

where $\mathbf{Q_{ij}}$ represents the stiffness matrix in principal axis. Changing the ply angle in each lamina influences the stiffness matrix $\mathbf{Q}$ as the material axis is not aligned with the laminate axis. Under fluid loading, the forces and moments experienced by the composite will be related to the strains at laminate level as:

$$\begin{bmatrix} N_x \\ N_y \\ N_{xy} \\ M_x \\ M_y \\ M_{xy} \end{bmatrix} = \begin{bmatrix} A_{11} & A_{12} & A_{16} & B_{11} & B_{12} & B_{16} \\ A_{12} & A_{22} & A_{26} & B_{12} & B_{22} & B_{26} \\ A_{16} & A_{26} & A_{66} & B_{16} & B_{26} & B_{66} \\ B_{11} & B_{12} & B_{16} & D_{11} & D_{12} & D_{16} \\ B_{12} & B_{22} & B_{26} & D_{12} & D_{22} & D_{26} \\ B_{16} & B_{26} & B_{66} & D_{16} & D_{26} & D_{66} \end{bmatrix} \begin{bmatrix} \epsilon_x \\ \epsilon_y \\ \gamma_{xy} \\ k_x \\ k_y \\ k_{xy} \end{bmatrix}$$

where N_x, N_y, N_{xy} are the fluid forces, M_x, M_y, M_{xy} are the fluid moments, k_x, k_y, k_{xy} are the laminate curvatures and

$$A_{ij} = \sum_{k=1}^{N} (\bar{Q}_{ij})_k t_k;\ i,j = 1,2,6 \quad (2)$$

represents the in=plane stiffness of the laminate (and presents values also for symmetric and balanced layups)

$$B_{ij} = \sum_{k=1}^{N} (\bar{Q}_{ij})_k t_k \bar{z}_k;\ i,j = 1,2,6 \quad (3)$$

represents the bending and/or extension coupling (i.e. the coupling term between moments and direct strains and forces and curvatures) and

$$D_{ij} = \sum_{k=1}^{N} (\bar{Q}_{ij})_k \left(t_k \bar{z}_k^2 + \frac{t_k^3}{12} \right);\ i,j = 1,2,6 \quad (4)$$

represents the bending stiffness of the component. In equations (2-4) k is the layer number and t_k is the thickness of the k^{th} layer. In equations (3-4) $\bar{z}_k$ is the distance from the mid-plane to the centroid of the k^{th} layer.

In order to correctly design tailored composite materials, it is necessary to account for the $\mathbf{B_{ij}}$ matrix as it gives the coupling terms for the bending-twist and extension-twist from the fluid-loads to the laminae structure.

3 EXPERIMENTAL SET-UP

The experiments were conducted in the 3.5 m × 2.4 m R. J. Mitchell closed circuit wind tunnel at the University of Southampton. Its turbulence intensity levels are less than 0.2% (Castro 2001). The investigated aerofoil is a NACA0015 section containing a load-carrying beam (that can be changed to investigate different ply angles), an aerofoil-shaped foam-rib structure and a layer of Mylar to transfer the aerodynamic loading to the foam and the beam, see Figure 1. The load-carrying beam is made of a sandwich structure (where the two skins are unidirectional carbon fibres and the core is Aluminium 6082).

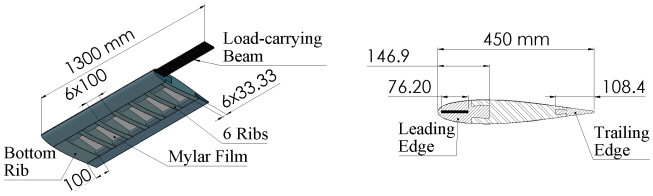

Figure 1: Tested specimen showing the load carrying carbon-aluminium beam, the foam-rib structure and the Mylar sheet as well as the principal dimensions.

This structure was chosen so that different fibres lay-up could be tested in the wind tunnel whilst maintaining the same aerodynamic shape. The structure is designed to be able to deflect more than 10% of its span length and to withstand the wind tunnel aerodynamic loadings for a Reynolds number (R_N) of 750,000, corresponding to the highest wind speed tested in the wind tunnel. The aerofoil dimensions are described in Table 1.

Table 1: PAC structure dimensions.

Parameter	Value	Dimension
Chord	450	[mm]
Span	900	[mm]
Aspect Ratio	2	
Thickness	67.5	[mm]
Area	40500	[mm^2]

The aerodynamic forces on the NACA0015 foil are measured via a six component Nuntem load

cell balance, mounted on a turntable in the roof of the wind tunnel. High-speed DIC is used to capture the structural response of the foil. Two SA3 Photron cameras were used with 100 mm Tokina lenses set with aperture of f-16. The speckle pattern, applied to a region of 450× 450 mm, was set to have a speckle size of approximately 7 pixels. This size allows each speckle to be described with reasonable confidence in the whole histogram intensity range, as described by Banks et al. (2015). The tip vortex core position is investigated with high resolution PIV. The results of the tip vortex position measured with PIV are presented in (Marimon Giovannetti et al. 2016).

A schematic view of the experimental set-up can be seen in Figure 2.

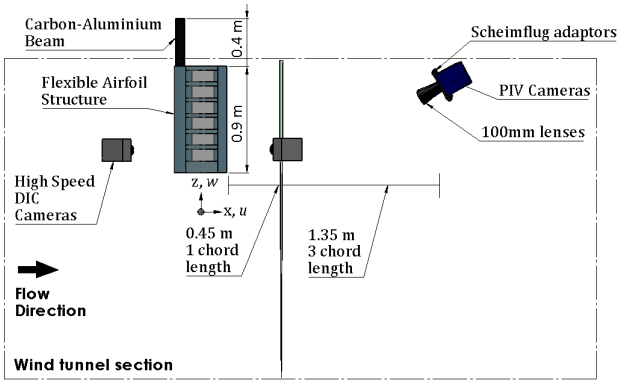

Figure 2: Side view schematic of the experimental set-up showing the principal dimensions and the used components. The coordinate system is shown at the balance centre around which the moments are measured.

During the wind tunnel experiments, three different beams were tested, one with no bend-twist coupling (i.e. $\phi = 0°$) and two Passive Adaptive Composite (PAC) beams of which one would resist the twist and one would enhance it (i.e. $\phi = -30°$and $\phi = 2 \times 30°$ respectively). Figure 3 presents the ply angle convention within the wind tunnel.

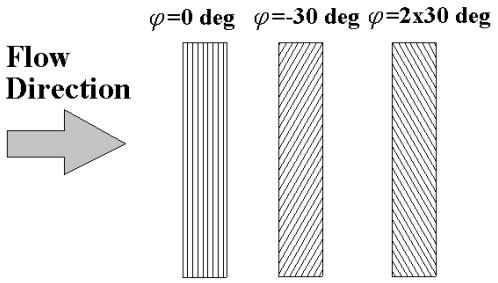

Figure 3: PAC beams ply angle convention.

4 NUMERICAL METHODOLOGY

A numerical model replicating the wind tunnel environment was developed. The aim was to provide a numerical prediction of the flexible composite structure response to fluid loading and comparing it with the experimental results. The numerical analysis was approached systematically, firstly assessing the validity of the FEA by applying to the structure a point load as measured in the experiments (i.e. at the centre of pressure location). Moreover, the full FSI simulation was assessed where the FEA model was put together with the CFD domain. The structural model was solved using the numerical software ABAQUS 6.13, coupled to Star-CCM+ 10.0.2 (that solves the flow) through the Co-Simulation Engine (CSE).

4.1 *FEA validation*

The finite element model of the aerofoil section closely represents the wind tunnel specimen. The material properties of the carbon, foam and Mylar were tested independently at the University of Southampton and are described in Table 2.

Table 2: Material properties of the wind tunnel and FEA models.

Material	Property	Value
Aluminium	ρ	2.7 e^{-9} tonne mm^{-3}
	E	55000 MPa
	ν	0.35
Carbon	ρ	3 e^{-9} tonne mm^{-3}
	E_1	117940 MPa
	$E_2 = E_3$	7840 MPa
	ν	0.25
	$G_{12} = G_{23}$	4400 MPa
	G_{13}	3600 MPa
Foam	ρ	3.6 e^{-12} tonne mm^{-3}
	$E_1 = E_2$	10.3 MPa
	E_3	5.5 MPa
	ν	0.3
	$G_{12} = G_{23} = G_{13}$	10.14 MPa
Mylar	ρ	2 e^{-9} tonne mm^{-3}
	E	2042.18 MPa
	ν	0.38

Figure 4 shows the mesh of the FEA model. In order to better describe bending, quadratic solid elements were used for the beam and foam parts. Shell elements were used to describe the Mylar behaviour, that, in order to correctly represent the flow around it, should present wrinkles on the compression side of the aerofoil in the FSI simulation. The total number of element size was approximately 58000. In order to correctly model the wind tunnel specimen the parts forming the aerofoil are joined together using tie-constraints and node-number similarity was ensured at intersection points, as can be seen in Figure 4. The FEA deflections and twists are compared to the data measured in the wind tunnel, as can be seen in Figure 5 and Figure 6 respectively. From both figures it is possible to see that the results lie within

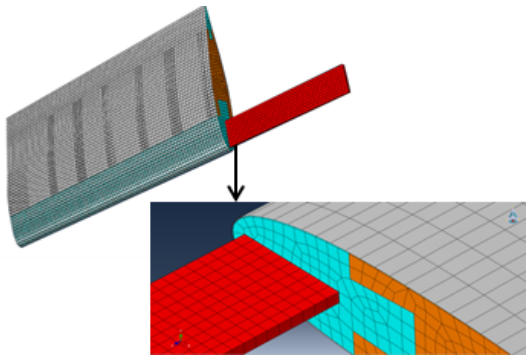

Figure 4: FEA mesh showing in different colours the different aerofoil components. The zoomed-in area shows the numbers of nodes similarities necessary at the intersection points.

the standard deviation error of the DIC measures for steady cases (i.e. when the angle of attack - α - is less than 13.7 degrees). For both deflection and twist results the standard deviation of DIC measures in steady case is extremely small (i.e. <0.5 mm for deflection measures and <0.02° for twist measures). In unsteady (stalled) conditions (α >13.7°) the FEA results follow the same trend of the DIC measures, but differ from them as only a static load is applied to the centre of pressure, therefore the unsteady condition is not reproduced in the numerical model.

The deflection curve follows the force measures, as after stall the lift force produced by the aerofoil drastically decreases and the drag forces increases, but the total force magnitude on the aerofoil decreases, leading to a smaller deflection.

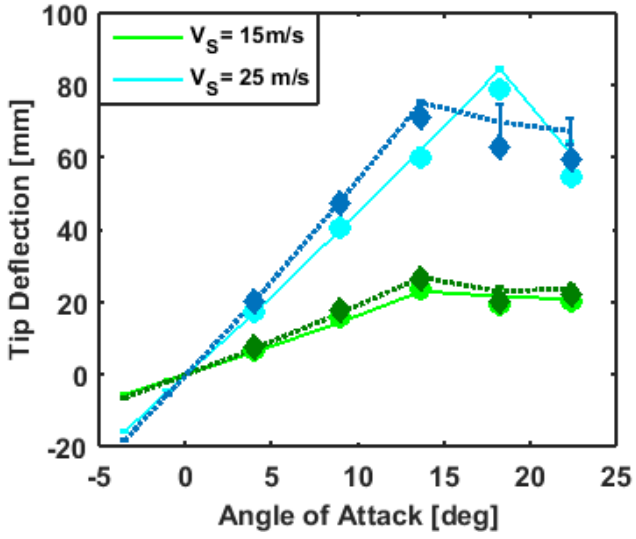

Figure 5: Tip deflection magnitude over angle of attack for two different wind speeds. The full-lines represent $\phi = 0°$ and the dotted lines represent $\phi = -30°$ measured in the experiments. The markers represent the FEA results for both $\phi = 0°$ (light-colours) and $\phi = -30°$ (dark colours).

It is interesting to note how the deflections are higher once a ply angle is introduced in the system (as expected due to a higher flexibility of the beam) but also how the negative ply angle resists the twist (Figure 6) naturally twisting the aerofoil section to a higher stall point (i.e. towards a positive change in angle of attack).

The FEA model is able to accurately predict the structural response when a fibre angle of $\phi = -30°$ is introduced, capturing the higher deflection and the change in angle of attack. The high standard deviation encountered near-stall in the $\phi = -30°$ case during the wind tunnel tests can be associated to the ply angle that induces a twist toward stall in increased pressures. The induced twist (toward a higher angle of attack) indicates that the stall-point of the $\phi = -30°$ aerofoil is reached at an angle between 13.7° and 18.3°, therefore the exact angle of stall is not measured.

4.2 *FSI validation*

Having assessed the validity of the FEA numerical model, it was possible to couple it inside the CFD domain. The CFD environment was also set to replicate closely the wind tunnel experiments, presenting the same dimensions of the working section of the wind tunnel in the y and z directions (i.e. width and height of the wind tunnel). The CFD mesh is formed of approximately 4.3 million cells with regions of refinement near the specimen, in the boundary layer (assuming a y^+ value in the turbulent region -i.e. y^+>50) and in the wake of the aerofoil. Moreover, the boundary conditions of the aerofoil were closely represented, fixing 350 mm of the beam section above the wind tunnel ceiling and leaving the aerofoil and 50 mm of the beam under the wind loads, as shown in Figure 2. Both simulations are set as dynamic implicit as the highly flexible model needs to be represented with a strongly coupled simulation in order to capture the small changes in deflections over time. In a time-accurate response the pressure and shear are exported from the CFD to the FEA analysis and the displacement and deformation are imported to the CFD from the FEA. A common physical interface surface is established in the two software: the aerofoil external shape plus the 50 mm of beam exposed to the wind. In this surface the pressures and shears are read in the CFD domain at the mesh-cell centre and the deflections are read in the FEA domain at the mesh-nodes. Therefore, a mapping between the two meshes is developed within the CSE to correctly apply the loads to the structure and the deformation in the fluid domain. The case presented corresponds to a wind speed V_S=14.95 m/s, angle of attack $\alpha = 9.97°$ and $\phi = 0°$. Figure 7 presents the FSI results for the side force and the deflections for both the numerical and experimental data. It has to be noted that the CFD domain is initiated to develop the flow around the aerofoil with the fixed geometry. Moreover, the aerofoil is released and it becomes free to move, leading to an initial overshoot in the deflection response. The

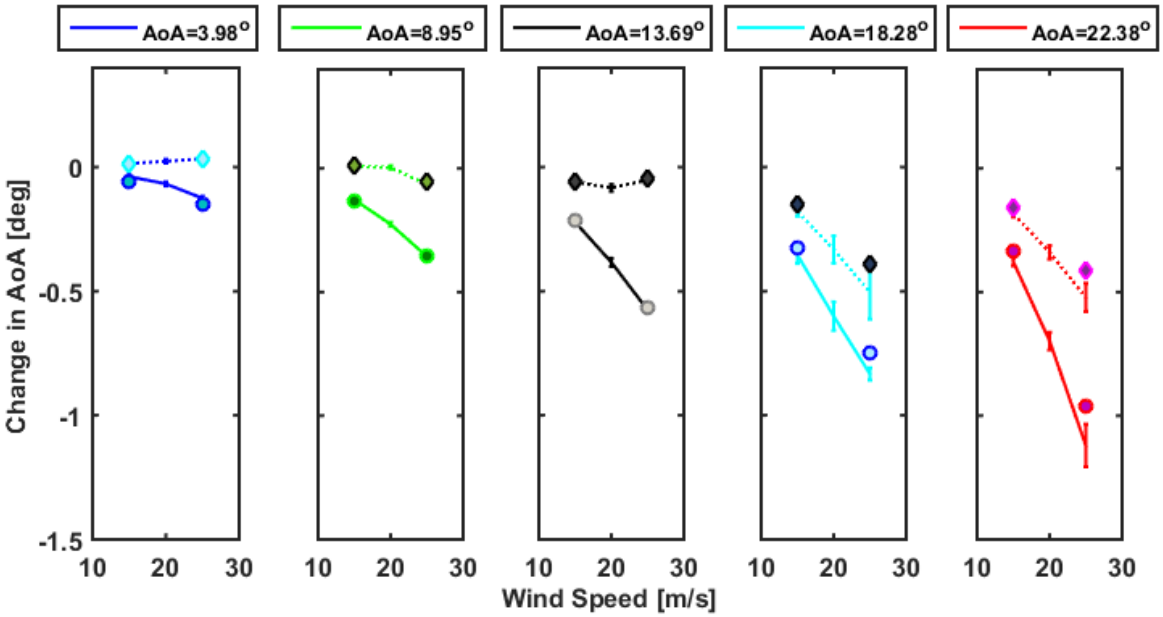

Figure 6: Change in angle of attack for different wind speeds and set-angles of attack. The full-lines represent $\phi = 0°$ and the dotted lines represent $\phi = -30°$ measured in the experiments. The markers represent the FEA results for both $\phi = 0°$ and $\phi = -30°$.

experimental data recording always began when the flow and hence the aerofoil reached a steady condition. Therefore the results are compared for t>2.5s, when the numerical simulation approaches a steady condition. Both the side force and the deflection show a good agreement between the experiments and the numerical simulations. The numerical simulation presents a deflection and a side-force 3.5% smaller than the experimental value.

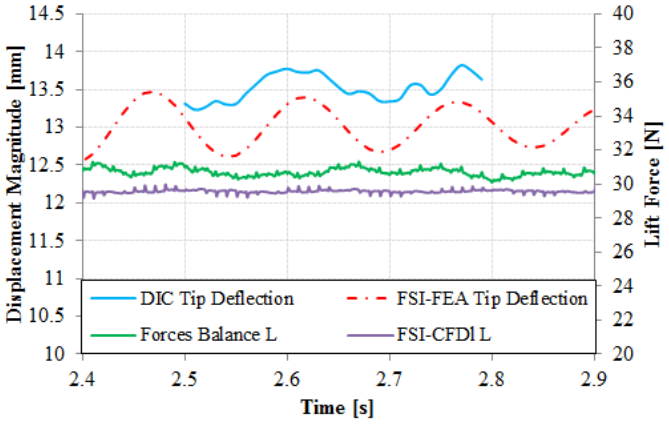

Figure 7: Deflection and lift force (L) over time for wind tunnel measures (i.e. deflection measured with DIC and lift by the forces balance) and FSI numerical simulations.

It is possible to see from the figure how the structural response is well represented by the numerical simulation not only in amplitude but also in period, leading to small oscillations at approximately 6.6 Hz, as recorded in the wind tunnel.

Figure 8 shows the comparison of twist angles at three different span-wise locations as measured with DIC and as modelled in the FSI simulation. It is possible to see that the FSI solution closely represents the DIC measures and the change in angle of attack experienced by the numerical aerofoil falls within the standard deviation of the DIC measures.

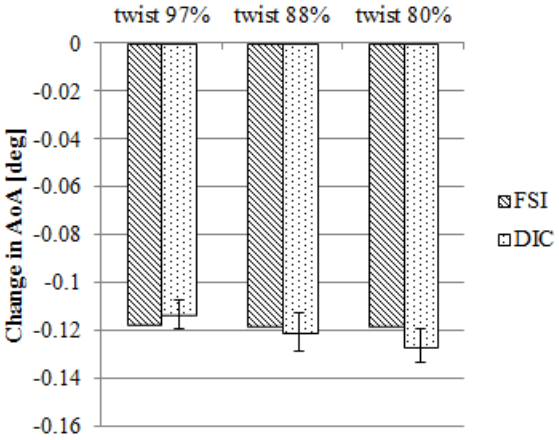

Figure 8: Twist angle comparison between DIC and FSI numerical simulations at three different span-wise locations.

5 CONCLUSIONS

Fluid structure interaction experimental and numerical methodologies are presented and compared. The lack of experimental data for aeroelastic problems triggered the necessity to provide a repeatable and robust experimental method that can be reproduced using DIC and PIV within a wind tunnel environment. Moreover, due to the complexity of numerical simulations that involve a full resolution of the CFD and FEA domains it was necessary to validate the numerical simulations comparing the results with wind tunnel measures. In order to ensure a correct resolution of both the FEA and the CFD this process was built in subsequent levels, investigating firstly the

structure on its own and its response to the loads experienced in the wind tunnel. A similar approach was ensured also for the CFD, not presented in the present study. The confidence acquired in the two separate systems lead to the possibility of coupling them to achieve reliable results for a complex engineering problem such as a FSI investigation. It was necessary to ensure that the results were accurate not only for a quasi-isotropic aerofoil, but also that the change in deflection and twist was captured for a Passive Adaptive Beam with a ply angle different from zero. The FEA model with loads applied at the center of effort in the three directions, as measured in the wind tunnel, ensured that it was possible to model correctly different beams inside a foam structure. The higher deflection and the resist in twist are seen not only during the experiments but also in the numerical simulations. Moreover, the complex FEA model was solved coupled with the CFD domain, so that the dynamic and inertia effects could be described under a realistic wind load. This approach showed that the forces and deflection experienced in the wind tunnel differed by 3.5% by the ones simulated and that the simulated twist lie within the standard deviation of the DIC measuring system. Moreover, the same change in deflection frequency is seen in both the experimental and numerical model. This study shows that it will be possible to use coupled FSI numerical simulations as a design tool to improve the performances of composite aerofoil-shaped sections. This can be achieved investigating not only the external geometry under load, but also the possibility of tailoring the internal structure to a given design loading condition.

AKNOWLEDGEMENT

The authors would like to acknowledge the EPSRC for funding this research under the grant number EP/I009876/1. The authors would also thank the University of Southampton, the members of the TSRL and Dave Marshall and his team in the R. J. Mitchell wind tunnel. Moreover, we would like to thank Dave Hollis from LaVision for his assistance in the DIC and PIV.

REFERENCES

Banks, J., L. Marimon Giovannetti, X. Soubeyran, A. M. Wright, S. R. Turnock, & S. W. Boyd (2015). Assessment of Digital Image Correlation as a method of obtaining deformations of a structure under fl uid load. *Journal of Fluids and Structures 58*, 173–187.

Barbero, E. J. (2008). *Finite Element Analysis of Composite Materials*. CRC Press.

Castro, I. P. (2001). Calibration tests in the working section of the R J Mitchell Wind Tunnel. Technical report, University of Southampton.

De Goeij, W. C., M. J. L. Van Tooren, & A. Beukers (1999). Implementation of bending-torsion coupling in the design of a wind-turbine rotor-blade. *Applied Energy 63*(3), 191–207.

Ducoin, A., J. André Astolfi, & J. F. Sigrist (2012). An experimental analysis of fluid structure interaction on a flexible hydrofoil in various flow regimes including cavitating flow. *European Journal of Mechanics, B/Fluids 36*, 63–74.

Fedorov, V. (2012). *Bend-Twist Coupling Effects in Wind Turbine Blades*. Ph. D. thesis, Technical University of Denmark.

Karaolis, N. M. (1989). The design of fibre reinforced composite blades for passive and active wind turbine rotor aerodynamic control. (October).

Malijaarsl, P. J. & M. L. Kaminski (2015). Hydro-elastic Analysis of Flexible Propellers: an overview. In *Fourth International Symposium on Marine Propulsors*, Austin.

Marimon Giovannetti, L., J. Banks, S. Turnock, & S. Boyd (2016). Uncertainty assessment of coupled Digital Image Correlation and Particle Image Velocimetry during wind tunnel experiments. Manuscript submitted for publication.

Nicholls-Lee, R., S. W. Boyd, & S. R. Turnock (2009). Development of high performance composite bend-twist coupled blades for a horizontal axis tidal turbine. In *17h International Conference on Composite Materials*.

Reddy, J. (2000). *Mechanics of Laminated Composite Plates and Shells* (2nd ed.). CRC Pess LLC.

Shirk, M. H., T. J. Hertz, & T. A. Weisshaar (1985). Aeroelastic Tailoring - Theory , Practice , and Promise. *23*(1).

Turnock, S. R. & A. M. Wright (2000). Directly coupled fluid structural model of a ship rudder behind a propeller. *Marine Structures 13*, 53–72.

Veers, P., S. N. Laboratories, G. Bir, N. Renewable, N. Wind, & D. Lobitz (1998). Aeroelastic Tailoring in Wind-Turbine Blade Applications. *Wind Energy* (1981).